2003

Synthesis and Characterization of MnO_2-Based Mixed Oxides as Supercapacitors

Hansung Kim
University of South Carolina - Columbia

Branko N. Popov
University of South Carolina - Columbia, popov@engr.sc.edu

Publication Info

Journal of the Electrochemical Society, 2003, pages D56-D62.

Journal of The Electrochemical Society, **150** (3) D56-D62 (2003)
0013-4651/2003/150(3)/D56/7/$7.00 © The Electrochemical Society, Inc.

Synthesis and Characterization of MnO_2-Based Mixed Oxides as Supercapacitors

Hansung Kim* and Branko N. Popov,z**

Center for Electrochemical Engineering, Department of Chemical Engineering, University of South Carolina, Columbia, South Carolina 29208, USA

Mn/Pb and Mn/Ni mixed oxide were prepared at ambient temperature by reduction of $KMnO_4$ with Mn, Pb, and Ni salts. This low-temperature approach provides amorphous structure of the active material. The specific capacitance of pure MnO_2 was estimated to be 166 F/g and increased to 210 and 185 F/g for Mn/Ni and Mn/Pb oxides, respectively. The carbon loading was optimized at 20 wt %. Based on a single electrode, the Mn/Ni mixed oxide showed a high rate capability of 3.12 Wh/kg at constant power discharge of 1 kW/kg.
 [DOI: 10.1149/1.1541675]

Manuscript submitted March 11, 2002; revised manuscript received August 22, 2002. Available electronically January 28, 2003.

The development of a high-power-density supercapacitor with a high energy density is one of the critical requirements for high-power-demanding electric devices such as an electric vehicle.[1-4] Amorphous nanostructured oxides, mixed metal oxides exhibiting pseudocapacitance are considered to be promising materials for high-energy-density power.[5-7] Amorphous $RuO_2 \cdot xH_2O$ prepared by sol-gel process was reported to have a capacitance of over 720 F/g.[8] However, the high cost of this material and low porosity, which causes depletion of the electrolyte absorbed in the electrode as well as the rapid decrease of power density observed at high charge/discharge rates, make this material inadequate for commercial applications.

Recent research is focused on increasing the utilization of ruthenium oxide and minimizing the ruthenium content by incorporating less expensive materials. Amorphous nanostructured materials with different RuO_2 loadings on carbon were prepared by the colloidal method.[9] The specific capacitance of $RuO_2 \cdot xH_2O$ was estimated to be approximately 863 F/g. Cao and Prakash synthesized Pb/Ru pyrochlore oxide ($Pb_2Ru_2O_{6.5}$).[10] The X-ray diffraction (XRD) of this material when heat-treated at 100°C showed a crystalline structure and a surface area measured using BET of 35 m^2/g. The capacitors built with these electrodes showed over 5 Wh/kg at 750 W/kg power level. Jeong and Manthiram[11] reported that ruthenium-chromium mixed oxides prepared by reduction of aqueous potassium dichromate solution with ruthenium chloride solution at pH 6.5 have better capacitance than pure RuO_2. Wilde *et al.*[12] suggested the perovskite type of strontium ruthenate $SrRuO_3$ as a pseudocapacitance material. They found that by replacing Sr with La and Mn, the capacitance of the active material increases significantly.

Attempts were also made to develop supercapacitors based on non-noble oxides.[13] Hydrous manganese oxide (a-$MnO_2 \cdot nH_2O$) was prepared by reduction of potassium permanganate with manganese acetate.[14] This active material in 1 M KCl aqueous electrolyte exhibits a capacitance of 153 F/g. Nickel oxide made by the sol-gel method[15] or electrochemical oxidation[16] was found to have a pseudocapacitance of 50-64 F/g (equivalent to 200 to 256 F/g for a single electrode). Sol-gel-derived cobalt oxide with a maximum capacitance of 291 F/g was also suggested as a supercapacitor material.[17] However, the operating potential window of these materials in KOH solution is below 0.6 V. Because the energy density depends on the square of the potential difference, the stability over large potential range is considered to be a crucial factor for supercapacitors.

In this study an attempt was made to synthesize at ambient temperature new mixed oxides based on MnO_2. Mn/Pb and Mn/Ni oxides were prepared by reduction of $KMnO_4$ with Mn, Pb, and Ni(II) salts. This low-temperature approach provides amorphous structure of the active material. The factors influencing the electrochemical performance of the electrode material were examined extensively.

Experimental

Mn/X (X = Pb or Ni) mixed oxides were synthesized by reduction of $KMnO_4$ with either lead(II) acetate-manganese acetate or nickel(II) acetate-manganese acetate reducing solutions, respectively.[18] The aqueous solution of $KMnO_4$ with a concentration of 0.17 M was prepared using distillated water. A controlled amount of $(CH_3CO_2)_2Mn$ salts and either lead(II) acetate or nickel(II) acetate were dissolved in distilled water to give a designed ratio between Mn and X. Next, the two solutions were mixed and stirred for 6 h at room temperature. The initial purple color of $KMnO_4$ changes to a dark brown with the initiation of the precipitation reaction. The precipitate, a dark powder, was filtered and washed several times with distilled water and annealed in a conventional oven. After annealing the filtrate, the oxides were mixed with 20 wt % carbon black (Black pearls 2000, Cabot Corp) and 5 wt %, poly(tetrafluoroethylene) (PTFE) and ground to form a paste. Pellet-type electrodes of 8 mm diam, weighing around 5 mg, were prepared by punching the paste and then cold pressed between two titanium grids. For comparison, amorphous manganese oxide was also prepared by the reduction of potassium permanganate with manganese acetate following the procedure reported in the literature.[14,18]

Electrochemical characterization studies of these electrodes were carried out using an EG&G PAR model 273A, Arbin battery tester and a conventional three-electrode setup. The 2.5 × 2.5 cm platinum plate and the saturated calomel electrode (SCE) were used as a counter and reference electrode, respectively. Cyclic voltammetry (CV) and galvanostatic charge-discharge studies were performed in 1 M Na_2SO_4 solution. The rate capability of the electrodes was evaluated at constant power discharge using the Arbin battery tester. The power density used to discharge the electrodes was in the range between 70 and 2000 W/kg.

XRD analysis (Rigaku 405S5 with Cu Kα as the radiation source) was carried out on the samples to examine the crystallinity of the material. The energy-dispersive analysis by X-ray (EDAX) was used to determine the composition of the mixed oxides. Surface area and pore volume of the electrodes were obtained by Brunauer-Emmett-Teller (BET) analysis using Nova 2000 (Quantachrome, Inc.). The weight loss of the material and the heat flow associated with the thermal decomposition were studied by thermogravimetric analysis (TGA) and differential thermal analysis (DTA).

Results and Discussion

Figure 1 shows CVs of MnO_2, Mn/Pb, and Mn/Ni mixed oxide electrodes obtained in 1 M Na_2SO_4 using a potential window be-

* Electrochemical Society Student Member.
** Electrochemical Society Active Member.
z E-mail: popov@engr.sc.edu

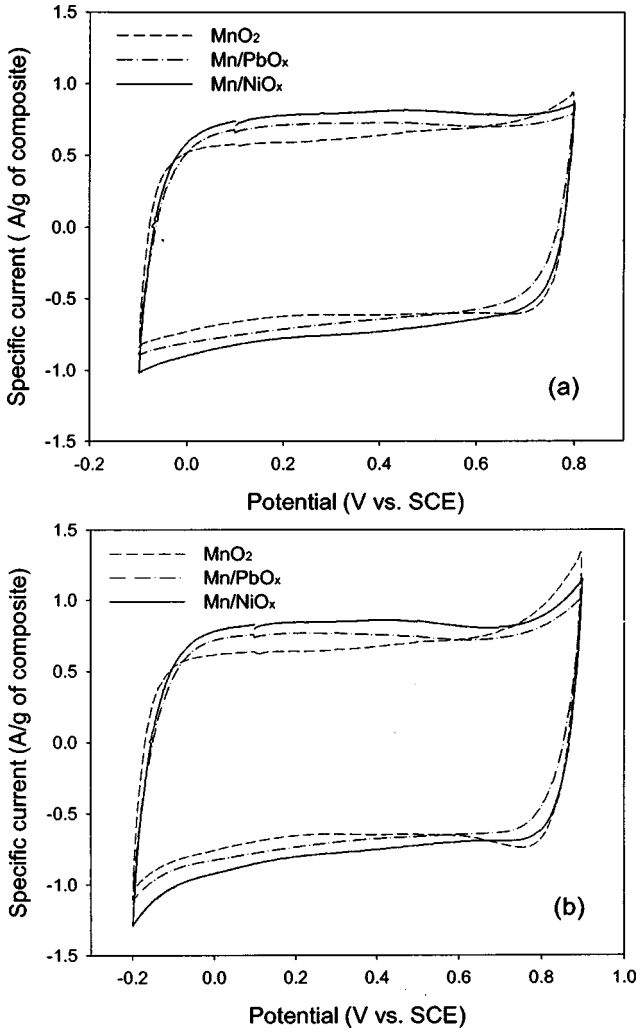

Figure 1. Cyclic voltammograms of MnO_2, Mn/PbO_x, and Mn/NiO_x obtained at a scan rate of 5 mV/s in 1 M Na_2SO_4: (a) potential range between −0.1 and 0.8 V *vs.* SCE and (b) potential range between −0.2 and 0.9 V *vs.* SCE.

tween −0.1 and 0.8 V *vs.* SCE. The shape of the voltammograms indicated a rectangular image corresponding to a typical capacitive behavior for all three materials. An increase of the specific current (A/g) of Mn/Pb and Mn/Ni mixed oxides was observed when compared with the specific current measured for pure MnO_2. Figure 1b shows an increase of the cathodic peak when the potential window is increased to −0.2 V *vs.* SCE. Since the thermodynamic potential of HER at pH 5 is −0.53 V *vs.* SCE, the observed increase of the cathodic current corresponds to reduction of the oxide from the composite electrode. The oxidation peak in Fig. 1b clearly shows that alloying MnO_2 with Pb and Ni reduces the peak current at −0.9 V. Since the equilibrium potential of oxygen evolution reaction (OER) is 0.69 V *vs.* SCE, the results indicate that the presence of Pb or Ni in the composite electrode increases the overpotential necessary for OER.

The specific capacitances of Mn/Ni and Mn/Pb mixed oxides are shown in Fig. 2 as a function of annealing temperature. The specific capacitances were estimated using a constant current discharge of 120 mA/g. The total capacitance of the composite is a sum of the pseudocapacitance of the transition metal oxide and the electric double-layer capacitance of carbon. Thus, in order to estimate the specific capacitance of the mixed oxides, it is necessary to subtract the electric double-layer capacitance of carbon from the total capacitance. The specific capacitance of pure carbon (Black pearls 2000) used in this study was estimated in 1 M Na_2SO_4 to be 70 F/g. This value is smaller than 216 F/g measured for the same carbon in H_2SO_4.[19] The observed difference can be explained by considering the ion sizes of Na^+ and H^+. Since Na^+ ion is larger than hydrogen proton, it occupies more active sites on the carbon surface than the proton, which lowers the total capacitance of the active material. The same phenomena was observed by Lee and Goodenough,[18] who found that the specific capacitance of RuO_2 measured in 2 M KCl is about 1/3 of the capacitance which has been estimated in 5.3 M H_2SO_4 solution.

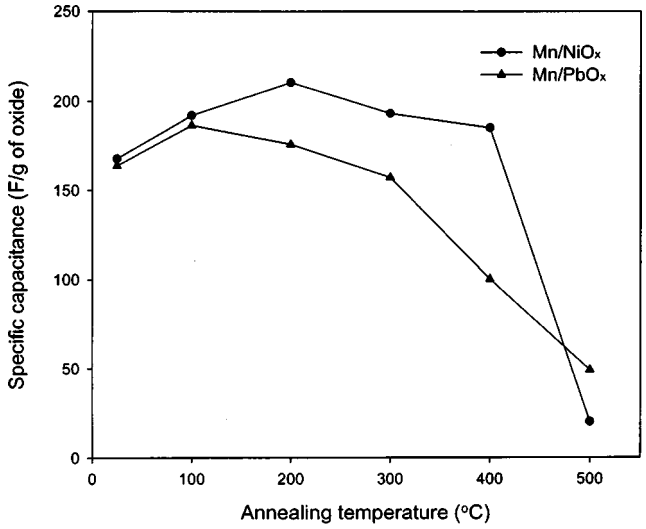

Figure 2. Effect of annealing temperature on the specific capacitance of Mn/PbO_x and Mn/NiO_x.

As shown in Fig. 2 the capacitance of Mn/Pb mixed oxide increases with increasing the annealing temperature and exhibits a maximum capacitance at 100°C. After reaching an annealing temperature of 100°C, the specific capacitance starts to decrease gradually. At temperatures higher that 400°C, a sharp decrease of the specific capacity was observed. Mn/Ni mixed oxide showed a similar behavior. The highest capacitance of 210 F/g was observed at approximately 200°C and it dropped drastically from 185 to 20 F/g at annealing temperature of 500°C. The pseudocapacitance depends on the water content in the oxides.[8,20] With increasing the water content, the ionic transport increases while the electronic transport decreases. Thus, in order to optimize the performance of the active material, it is necessary to optimize the water content in the oxide by a proper annealing process.

The XRD patterns of both $MnNi_{0.25}O_x$ and $MnPb_{0.25}O_x$ mixed oxides as a function of annealing temperature are given in Fig. 3. Broad diffraction peaks were observed for $MnPb_{0.25}O_x$ samples annealed at temperatures lower than 300°C, indicating the presence of an amorphous or nanocrystalline phase. Transmission electron microscopy (TEM) will be used in our future studies to clarify this issue. Upon increasing the temperature above 400°C, the width of the peaks starts to decrease, indicating that the structure changes to crystalline. In contrast to the $MnPb_{0.25}O_x$, the $MnNi_{0.25}O_x$ shows a sharp transition from amorphous to crystalline structure with increasing annealing temperature. At lower temperature than 400°C, this material exhibits an amorphous structure. At 500°C sharp diffraction peaks were detected, indicating a fully developed crystalline structure. This trend is in agreement with the observed decrease of the capacitance with increasing annealing temperature shown in Fig. 2. The results indicated that the capacitance strongly depends on the structure of the active material, which is controlled with the annealing temperature.

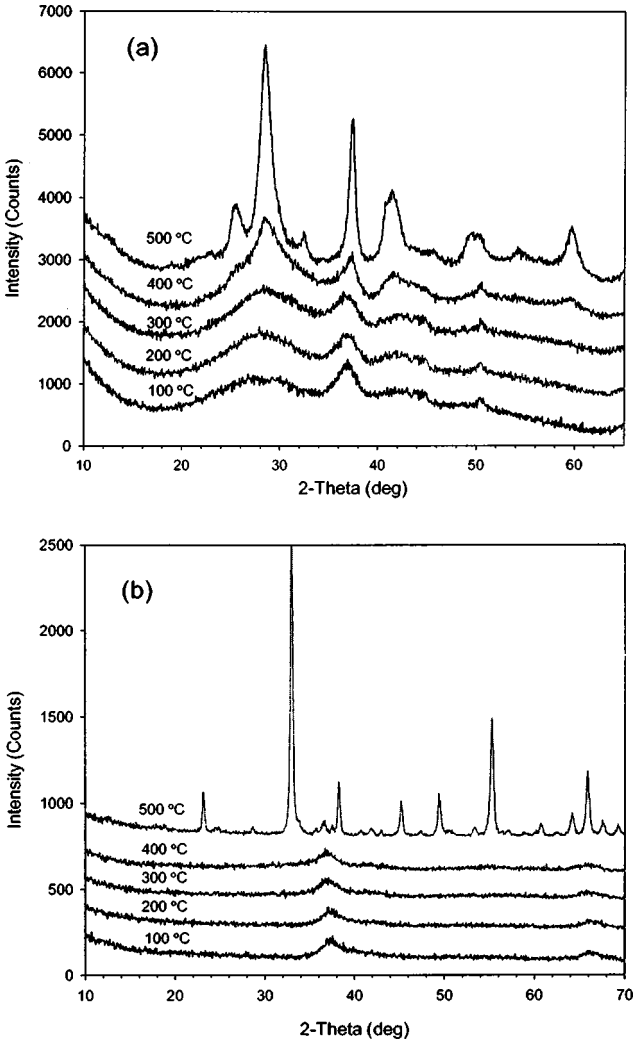

Figure 3. XRD patterns of (a) Mn/PbO_x and (b) Mn/NiO_x as a function of annealing temperature. The ratio of Mn/X is 8:2.

Figure 4 shows diffractions patterns of $MnPb_{0.25}O_x$ and $MnNi_{0.25}O_x$ annealed at 500°C. The XRD peaks of $MnPb_{0.25}O_x$ were identified using reference data as $Mn_8Pb_2O_{16}$. Note that the Mn to Pb ratio of 8:2 is the same with the composition of the metal ions used in the reaction solution to synthesize the Mn/Pb mixed oxide. The XRD peaks of $MnNi_{0.25}O_x$ annealed at 500°C corresponded mainly to Mn_2O_3 and $MnNiO_3$, which are electrochemically inactive materials. Thus, the results obtained in this study indicated that the electrochemical activity of $MnNi_{0.25}O_x$ diminishes at high annealing temperature due to separation of the active material into crystalline Mn- and Ni-rich phases by diffusion.

Figure 5 shows the TGA and DTA results obtained for Mn/Pb and Mn/N mixed oxide at a constant heating rate of 10°C/min in an atmosphere of He gas. A continuous weight loss resulting from the dehydration of the adsorbed and the lattice water is observed for both samples. Strong endothermic peaks were also observed below 100°C due to a loss of water which was physically adsorbed. As temperature increases, only Mn/Ni mixed oxide shows another small but sharp weight loss and an endothermic peak caused by the loss of oxygen at approximately 500°C. This temperature coincides with the temperature where clear structural and phase transitions were observed in Fig. 3 and 4. Based on these results, it is reasonable to assume that both the change in the crystalline structure and the mixed oxide decomposition process contribute to sharper decrease of capacitance in the case of Mn/Ni mixed oxide.

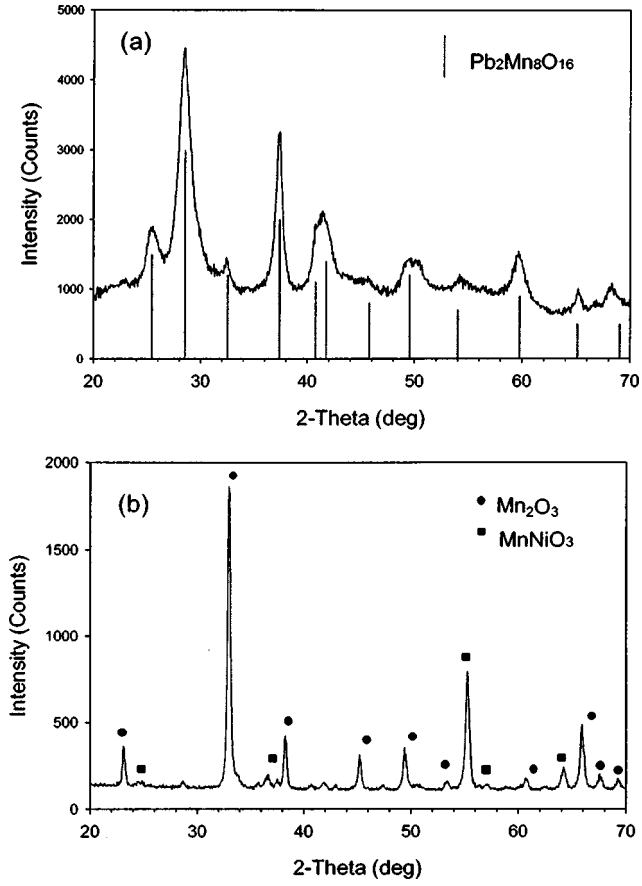

Figure 4. XRD patterns of (a) Mn/PbO_x and (b) Mn/NiO_x annealed at 500°C.

Figure 6a shows the results from EDAX elemental analysis of Mn/Pb and Mn/Ni mixed oxides prepared by using different initial concentrations of metal ions in the solution. EDAX analysis is a technique which provides a semiquantitative estimate of the surface elements. If the reaction proceeds completely, the detected composition of each component should be on the diagonal line of the graph with the percentage ratio of Ni or Pb to Mn used to synthesize the mixed oxide. In case of Pb, almost a linear relationship between used and detected ratio exists until Pb reaches 20 mol %. In the case of Mn/Ni mixed oxides, Ni is not well mixed with Mn when compared to Mn/Pb mixed oxide. Figure 6b presents the dependence of the specific capacitance on the Ni/Mn and Pb/Mn ratio. The pure MnO_2 has a specific capacitance of 166 F/g. With increasing the ratio of Pb and Ni, the specific capacitance goes through a maximum at approximately 20 mol % Ni or Pb. The specific capacitance was estimated to be 210 and 185 F/g for Mn/Ni and Mn/Pb mixed oxides, respectively. Since Pb has a very high density, a high Pb content in the mixed oxide is not favorable in obtaining a material with high specific capacitance.

In order to estimate if any change of the physical structure occurs due to incorporation of Ni into MnO_2, the specific surface area and the pore size distribution were estimated using multipoint Brunauer-Emmett-Teller (BET) analysis. As shown in Fig. 7, pure MnO_2 has a specific surface area of 165 m^2/g. The pore size is in the range between 70 and 100 Å. In case of a mixed Mn/Ni oxide with 10 mol % Ni, the specific surface area increases to 185 m^2/g. The portion with a pore size which was in the range between 70 and 100 Å of MnO_2 decreased while the portion with a pore size of 20 Å increased. The pore size of Mn/Ni mixed oxide with 20 mol % Ni in the mixed oxide shifted completely to 20 Å while the specific surface area of this material increased to 207 m^2/g. Therefore, the ob-

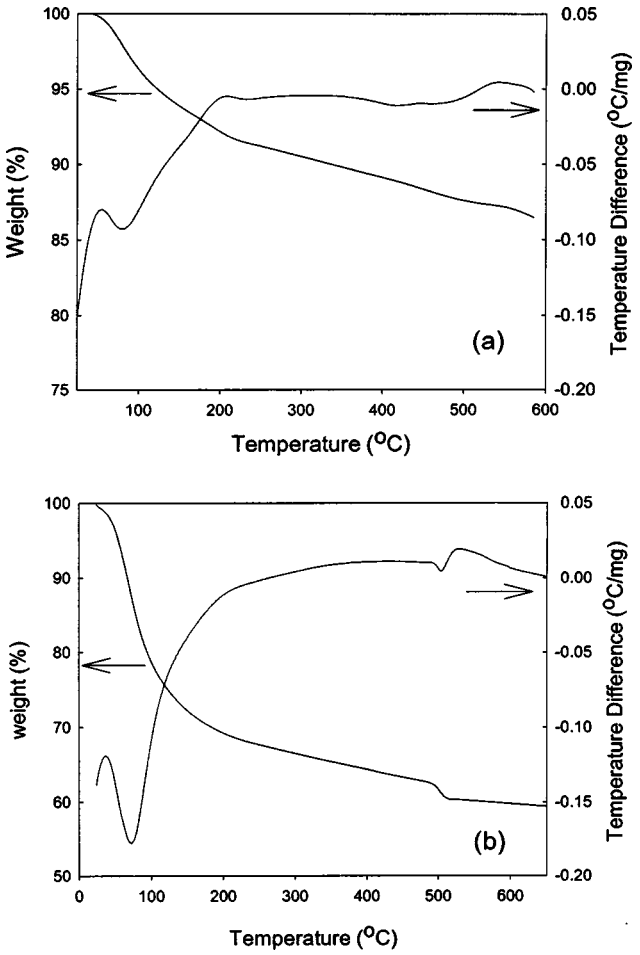

Figure 5. TGA and DTA of Mn/PbO_x and (b) Mn/NiO_x in He gas at 10°C/min. The ratio of Mn/X is 8:2.

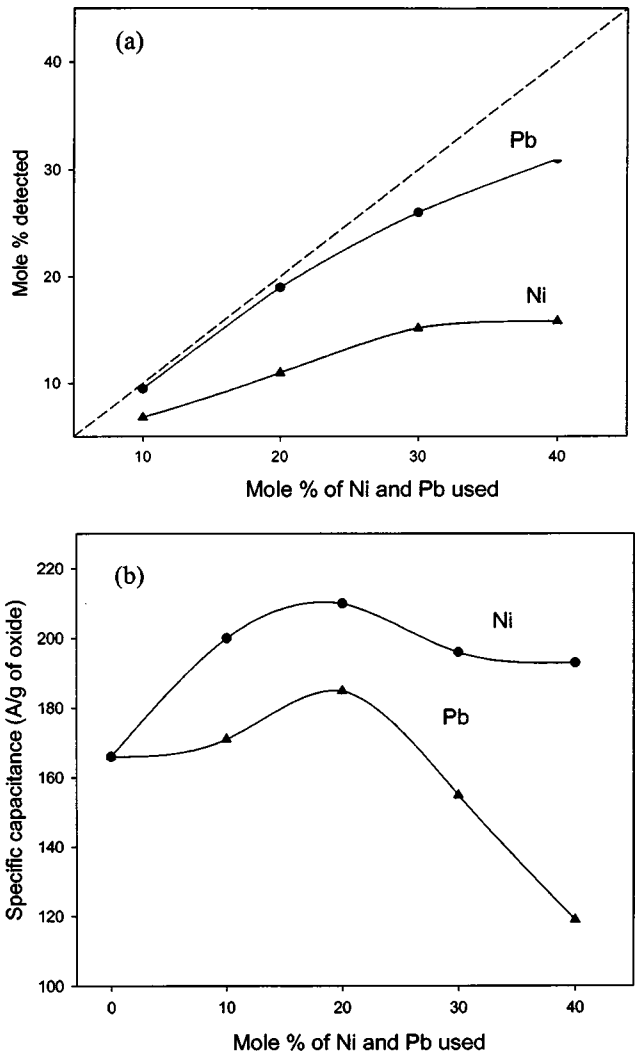

Figure 6. (a) Compositional analysis of Pb and Ni in mixed oxides using EDAX and (b) the specific capacitance corresponding to each composition.

served increase of surface area results from a formation of micropores accessible for the electrolyte, resulting in an increase of the capacitance of the mixed oxide when compared with the capacitance of pure MnO_2.

Since Mn-based materials have low conductivity, the content of the conducting material such as carbon included in the electrode is critical in obtaining a material with high electrochemical performance. Figure 8 shows cyclic voltammograms of Mn/Ni mixed oxide prepared with a different carbon loading. The binder content was fixed at 5 wt %. As shown in Fig. 8, upon increasing the carbon ratio from 5 to 20 wt %, the CVs indicated a typical capacitor behavior and became rectangular in shape. Also, the current response when the sweep direction changed became faster, indicating a decrease of the electrode resistance. Presence of carbon in the active material up to 20 wt % creates an electric path between the oxide particles, thus increasing the number of active sites for the electrochemical faradaic reaction.[14] As shown in Fig. 8, by increasing the carbon ratio above 20 wt %, the shape of the CV did not change significantly. In order to explain the effect of carbon content in the composite, the BET and the capacitance data as a function of carbon loading are summarized in Table I. The internal resistance was calculated based on the initial potential drop at constant current discharge of 120 mA/g. When the carbon loading is increased to 20 wt %, the value of the internal resistance decreases. However, no significant change of the resistance was observed with further increase of the carbon content in the mixed oxide. The measured BET and the pore volume of electrodes also increased with increasing the carbon loading because the specific surface area of carbon is approximately

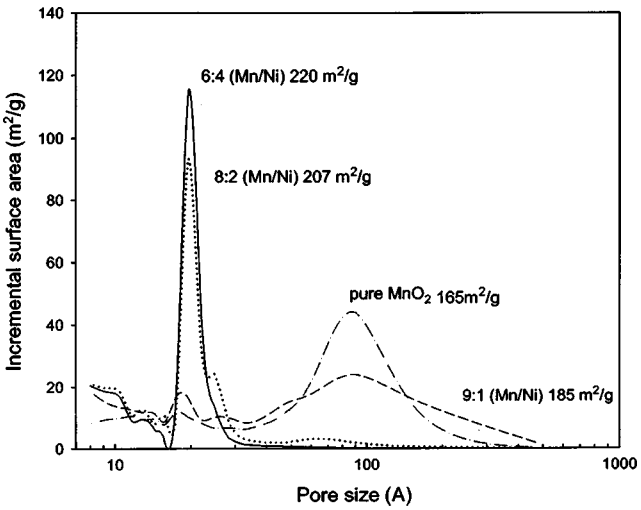

Figure 7. BET surface area and pore size distribution of Mn/NiO_x for different Ni loadings.

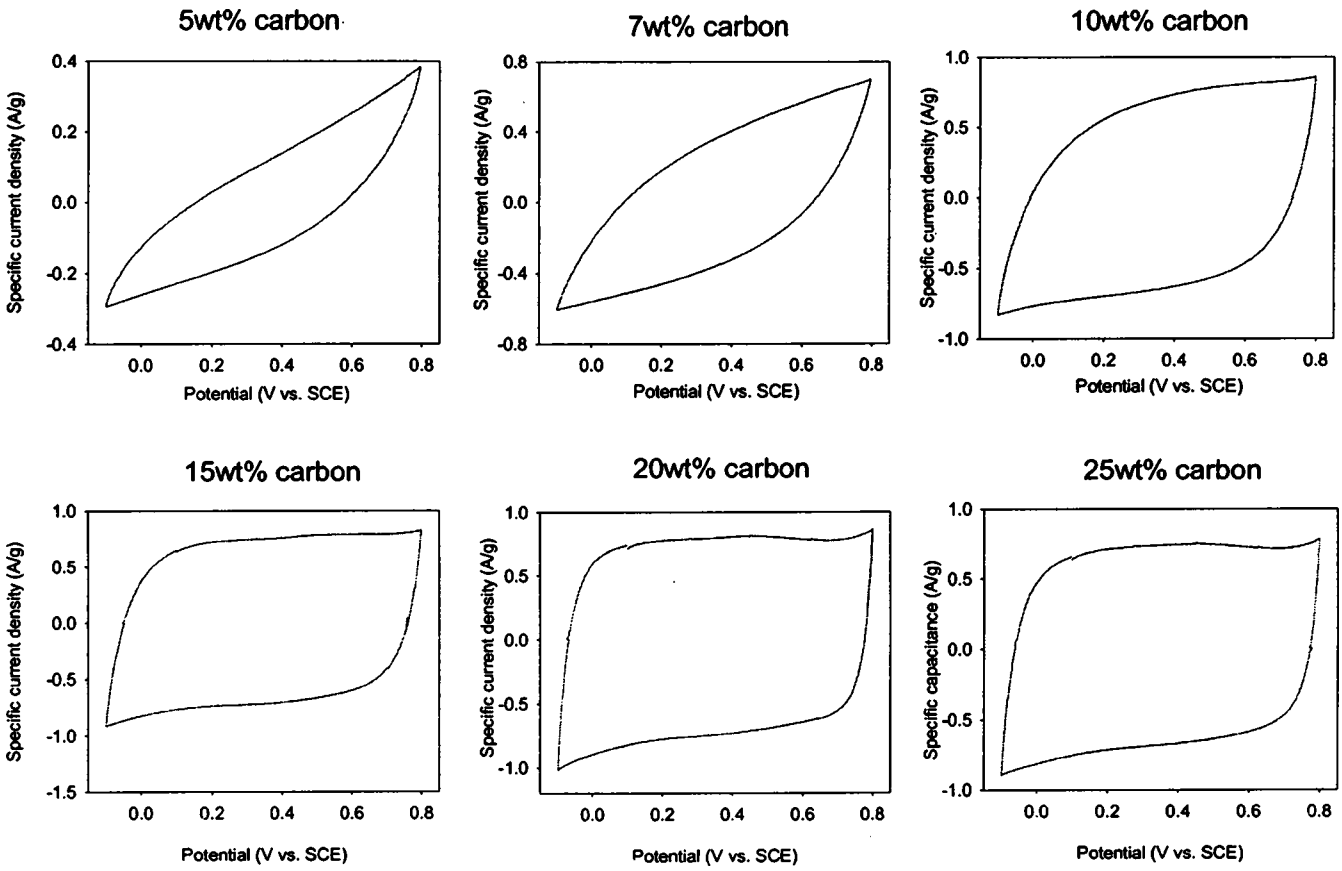

Figure 8. CVs of Mn/NiO_x as a function of carbon content in the electrode in 1 M Na_2SO_4 solution; potential range between −0.1 and 0.8 V *vs.* SCE and scan rate 5 mV. The ratio of Mn/Ni is 8:2.

1380 m^2/g, which is much higher than the Mn/Ni mixed oxide surface area of 207 m^2/g. Note that the specific capacitance increases until the carbon loading becomes 20 wt % and starts to decrease for loading higher than 20 wt %. The results can be explained by taking into account that carbon black used in this study has a smaller capacitance than Mn/Ni mixed oxide. Thus, as shown in Table I, the initial increase of the specific capacitance results from an increase of the conductivity of the electrode. When the carbon loading is higher than 20 wt %, the specific capacitance starts to decrease because the conductivity of the electrode reaches a steady-state value. Zheng also reported that mixing high porous carbon with RuO_2 improves the rate capability of the electrode. Unlike Mn-based mixed oxide, RuO_2 has a low electric resistance (10^{-3} Ω cm[19,21]). The high porous carbon included in the electrode acts like a reservoir and prevents the depletion of the electrolyte in the electrode when high-current-discharge modes are used.[22]

A Ragone plot of Mn/Ni mixed oxide as a function of carbon loading is shown in Fig. 9. At low carbon loading up to 5 wt %, the energy density is almost zero. Also, the mixed oxide shows very poor rate capability. With increasing the carbon content in the composite up to 20 wt %, the rate capability increased dramatically. However, it starts to decrease for higher carbon contents due to a decrease of the specific capacitance of the composite electrode.

The discharge energy density curves for MnO_2, Mn/Pb, and Mn/Ni mixed oxides obtained at constant power discharge of 1 kW/kg are shown in Fig. 10. The carbon content was fixed at 20 wt %. It is evident from the data that by incorporating MnO_2 with Ni and Pb, the energy density increased for more than 80%, which indicates that the rate capability of the electrode increases.

The stability of the active material in the electrolyte was tested using a CV. As shown in Fig. 11 approximately 3.2 and 4.4% loss of capacity was observed after 1000 cycles for Mn/Ni and Mn/Pb mixed oxide, respectively. Thus, a very stable material has been synthesized using the redox reactions described in this paper.

Table I. BET and capacitance of $MnNi_{0.25}O_x$ as a function of carbon loading.

Carbon content (wt %)	Specific capacitance (F/g of composite)	Specific capacitance (F/g of oxide)	BET (m^2/g)	Pore volume (10^{-3} mL/g)	Resistance (Ω)
5	44.9	46.1	227	345	1.48
7	111.5	121.1	273	397	1.18
10	152.5	171.2	286	441	0.35
15	161.1	188.3	338	523	0.21
20	171.9	210.5	387	601	0.15
25	163.3	208.3	541	642	0.15
30	155.5	206.9	596	725	0.13

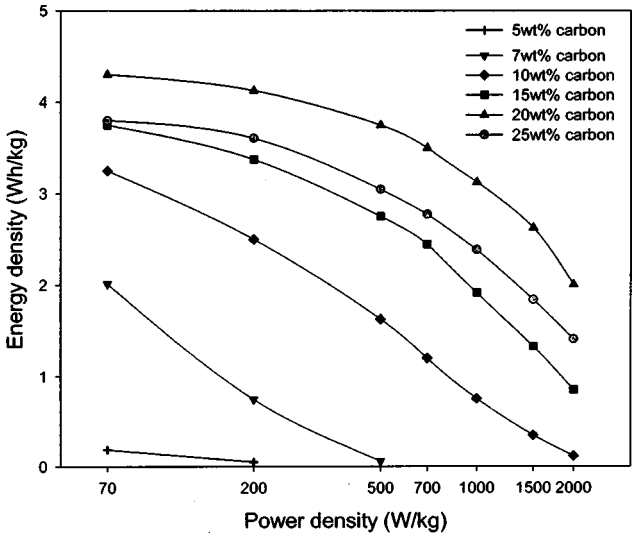

Figure 9. Ragone plot obtained for Mn/NiO_x electrodes as a function of carbon loading. The ratio of Mn/Ni is 8:2.

Conclusion

Mn/Pb and Mn/Ni mixed oxides were successfully synthesized by reduction of $KMnO_4$ with Mn, Pb, and Ni salts. By introducing Ni and Pb into MnO_2, the surface area of the mixed oxide increased due to a formation of micropores. The specific capacitance increased from 166 F/g estimated for MnO_2 to 210 and 185 F/g for Mn/Ni and Mn/Pb mixed oxides, respectively. It was found that the annealing temperature is strongly related to the capacitance of the active material. A transition from amorphous to a crystalline structure as well as decomposition of the active material at temperatures higher that 400°C account for the observed decrease of the specific capacitance. Carbon was used to increase conductivity of the electrode. The carbon loading was optimized at 20 wt %. At this loading, the Mn/Ni mixed oxide showed the highest rate capability of 3.12 Wh/kg at constant power discharge of 1 kW/kg.

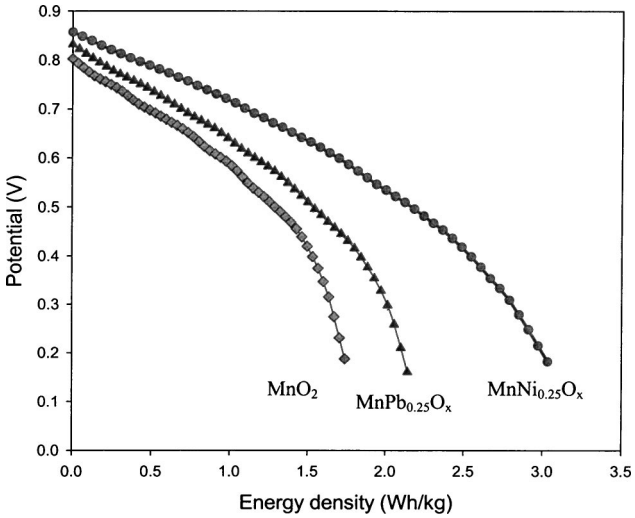

Figure 10. Discharged energy density curves of MnO_2, Mn/Pb, and Mn/Ni mixed oxides obtained at the constant power discharge of 1 kW/kg. The ratio of Mn/X is 8:2 and carbon ratio is 20 wt %.

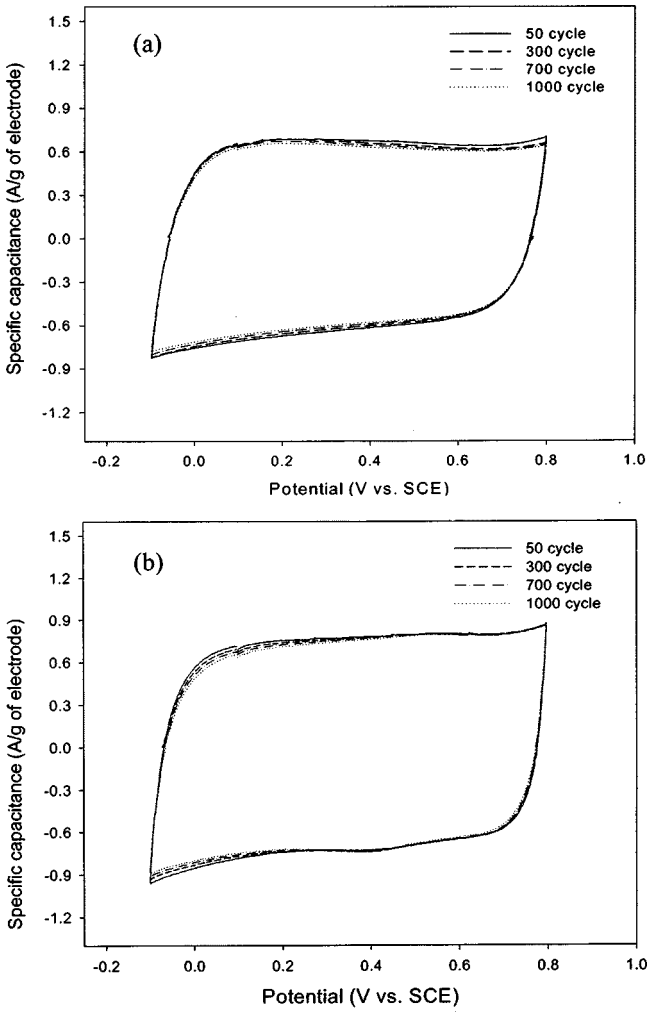

Figure 11. Cycle life tests of (a) Mn/PbO_x and (b) Mn/NiO_x in 1 M Na_2SO_4 solution. Potential range between −0.1 and 0.8 V *vs.* SCE and scan rate 5 mV/s. The ratio of Mn/X is 8:2.

Acknowledgments

The authors are grateful for the financial support by the Commission on Higher Education Fund no. 15510-G112 and for financial support provided by the National Reconnaissance Organization (NRO) under contract no. NRO-00-C-0134.

The University of South Carolina assisted in meeting the publication costs of this article.

References

1. A. F. Burke, *Hybrid/Electric Vehicle Design Options and Evaluation*, SAE paper no. 920447 (Feb 1992).
2. L. P. Jarvis, T. B. Atwater, and P. J. Cygan, *J. Power Sources*, **79**, 60 (1999).
3. G. Gutmann, *J. Power Sources*, **84**, 275 (1999).
4. A. F. Burke and T. C. Murphy, *Mater. Res. Soc. Symp. Proc.*, **393**, 375 (1995).
5. B. E. Conway, *J. Electrochem. Soc.*, **138**, 1539 (1991).
6. B. E. Conway, V. Birss, and J. Wojtowicz, *J. Power Sources*, **66**, 1 (1997).
7. J. P. Zheng and T. R. Jow, *J. Electrochem. Soc.*, **142**, L6 (1995).
8. J. P. Zheng, P. J. Cygan, and T. R. Jow, *J. Electrochem. Soc.*, **142**, 2699 (1995).
9. H. Kim and B. N. Popov, *J. Power Sources*, **104**, 52 (2002).
10. F. Cao and J. Prakash, *J. Power Sources*, **92**, 40 (2001).
11. Y. U. Jeong and A. Manthiram, *Electrochem. Solid-State Lett.*, **3**, 205 (2000).
12. P. M. Wilde, T. J. Guther, R. Oesten, and J. Garche, *J. Electroanal. Chem.*, **461**, 154 (1999).
13. S. Sarangapani, B. V. Tilak, and C. P. Chen, *J. Electrochem. Soc.*, **143**, 3791 (1996).
14. H. Y. Lee, S. W. Kim, and H. Y. Lee, *Electrochem. Solid-State Lett.*, **4**, A19 (2001).
15. K. C. Liu and M. A. Anderson, *J. Electrochem. Soc.*, **143**, 124 (1996).
16. V. Srinivasan and J. W. Weidner, *J. Electrochem. Soc.*, **144**, L210 (1997).

17. C. Lin, J. A. Ritter, and B. N. Popov, *J. Electrochem. Soc.*, **145**, 4097 (1998).
18. H. Y. Lee and J. B. Goodenough, *J. Solid State Chem.*, **144**, 220 (1999).
19. J. P. Zheng and T. R. Jow, U.S. Pat. 5,961,887 (1999).
20. D. A. Mckeown, P. L. Hagans, L. P. L. Carette, A. E. Russell, K. E. Swider, and D. R. Rolison, *J. Phys. Chem. B*, **103**, 4825 (1999).
21. K. Kinoshita, *Carbon: Electrochemical and Physicochemical Properties*, p. 76, John Wiley & Sons, New York (1988).
22. J. P. Zheng, *Electrochem. Solid-State Lett.*, **2**, 359 (1999).